5G PPP
PUBLIC-PRIVATE PARTNERSHIP

European Commission | Horizon 2020 European Union funding for Research & Innovation

5G-XHaul

Dynamically Reconfigurable Optical-Wireless Back-haul/Fronthaul with Cognitive Control Plane for Small Cells and Cloud-RANs

D4.12 Advanced Antenna System with Integrated L1 Processing

This project has received funding from the European Union's Framework Programme Horizon 2020 for research, technological development and demonstration

Advanced 5G Network Infrastructure for the Future Internet

Project Start Date: July 1st, 2015 Duration: 36 months

H2020-ICT-2014-2 671551 December 31st, 2016 – Version 1.0

Project co-funded by the European Commission

Under the H2020 programme

Dissemination Level: Public

Grant Agreement Number:	671551
Project Name:	Dynamically Reconfigurable Optical-Wireless Backhaul/Fronthaul with Cognitive Control Plane for Small Cells and Cloud-RANs
Project Acronym:	5G-XHaul
Document Number:	D4.12
Document Title:	Advanced Antenna Systems for Radio Access with Integrated L1 Processing
Version:	0.1
Delivery Date:	December 31st, 2016
Responsible:	**AIR**
Editor(s):	Albrecht Fehske (**AIR**)
Authors:	Albrecht Fehske, Michael Grieger (**AIR**), Jay Kant Chaudhary, Jens Bartelt (**TUD**)
Keywords:	Advance Antenna Systems, Active Elements, CPRI, Fronthaul, Backhaul, Functional Split
Status:	Draft
Dissemination Level	Public
Project URL:	http://www.5g-xhaul-project.eu/

Table of Contents

List of Figures

List of Tables

Executive Summary

5G-XHaul aims at building up an ambitious converged optical and wireless network solution that relies on a flexible infrastructure able to support backhaul (BH) and fronthaul (FH) networks required to cope with the future challenges imposed by 5G radio access networks. One of the key 5G access technologies is massive MIMO, which utilizes hundreds or even thousands of transceivers at a single radio unit to provide very high cell capacities and user throughputs. This technology, however, comes at the price of significantly higher data rate requirements on the FH link between the baseband and the radio unit compared to state-of-the-art radio units with only two or four transceivers.

In order to mitigate these requirements 5G-XHaul develops an advanced antenna system for massive MIMO, which features 96 transceivers and digital processing capabilities to support a specific functional split architecture that reduces the FH data rate requirements by a factor of six to twelve, depending on the number of virtual ports employed. In addition, 5G-XHaul develops a 5G base band unit (BBU) prototype platform. Here, the focus is on demonstration and evaluations of signal waveforms with the capability to reduce peak-to-average-power (PAPR) as well out-of-band (OOB) emissions significantly compared to state-of-the-art OFDM waveforms as used in LTE. The BBU implements generalized frequency division multiplexing (GFDM) as one promising candidate of such a waveform.

This report provides an overview of the concept, implementation, and performance of these two 5G-XHaul hardware platforms, i.e., the 5G BBU and the 5G advanced antenna system (AAS). Initial tests and measurements are performed on both platforms. These include OOB performance of the GFDM waveform generated by the BBU and RF performance such as adjacent channel leakage ratio (ACLR) and error vector magnitude (EVM) of the AAS. The performance results of both platforms meet regulatory requirements as well as expectations.

The implementation activities reported here contribute directly to the 5G-XHaul's ambition to demonstrate key enabling technologies for flexible and re-configurable transport networks for 5G mobile communications. A brief outline of corresponding demonstration activities as planned is given at the end of the report.

1 Introduction

The introduction of new access technologies in 5th generation radio networks has a considerable impact on the design of transport networks. Especially massive multiple-input/multiple output (MIMO) technologies with arrays of hundreds of transceivers will increase fronthaul (FH) data rates considerably. Since the currently dominant fronthaul standard, the common public radio interface (CPRI), defines the transport of one FH data stream per transceiver, the FH data rates for massive MIMO increase hundredfold. Accordingly, 5G-XHaul's WP 4 investigates innovative transport technologies both in the wireless and optical domain to support 5G *transport*. Within WP4, Task 4.3.2 investigates how to design antennas and remote radio heads (RRH) in an integrated way, in order to reduce the data rate requirements that transport technologies have to fulfil.

5G-XHaul develops an advanced antenna system (AAS) prototype, which includes not only the actual radiating elements and RF processing as conventional passive antennas and, respectively RRHs do. It also includes a subset of the digital physical layer processing, also called L1 processing, which is normally performed in the BBU. The 5G-XHaul prototype AAS features 96 transceivers in a modular design. By moving some of the L1 processing to the antenna the data rate requirements on the transport are reduced by a factor of 6-12, depending on the number of ports used at the AAS. The 5G-XHaul AAS goes beyond a mere massive MIMO proof-of-concept or research platform in that it features an industry-standard form factor, power consumption, and the aforementioned much slimmer digital interface to the base band.

Furthermore, 5G-XHaul develops a 5G BBU prototype platform. Here, the focus is on demonstration and evaluations of signal waveforms with the capability to reduce PAPR as well OOB emissions significantly compared to state-of-the-art OFDM waveforms as used in LTE. The BBU implements GFDM as one promising candidate of such a waveform. The BBU includes a full PHY layer stack as well as parts of the MAC layer for both transmission and reception. It is implemented on a software defined radio (SDR) hardware platform and will, among others, be used to provide baseband samples to the AAS for transmission. Combined with the AAS this will help to evaluate and verify the fronthaul transport of 5G waveforms.

The overall goal of these activities is a joint demonstration of BBU and AAS prototypes showing the feasibility of these key 5G technologies.

Concept, design, and initial test of these 5G-XHaul hardware developments are reported in this deliverable. Section 2 briefly reviews the additional challenges that massive MIMO introduces on the transport network. Section 3 provides the hardware concepts and architecture of both the BBU and the AAS. Section 4 gives initial test results of both hardware platforms. Section 5 outlines the planned integration of both platforms into the 5G-XHaul testbed.

2 Fronthaul challenges of massive MIMO

Massive MIMO [1] is one of the most promising technologies considered for 5G networks in order to dramatically increase the radio access capacity in future mobile networks. Massive MIMO employs large number of antenna elements (e.g. hundreds or even thousands) at radio access points to simultaneously serve several users (e.g. tens or hundreds) in the same time frequency resource. These antennas improve the signal reception at the desired destination by focusing the radiated energy into even smaller regions of space. By digital or analogue manipulation of the signal phases of the different antenna elements, transmit power can be focused in defined direction, thereby overcoming path loss and separating users spatially, both leading to an increase in radio access data rates. Theoretic studies suggest an increase in spectral efficiency of up to 10 [1] compared to conventional systems, and a prototype developed by the 5G-XHaul Partner UNIVBRIS achieved a throughput of up to 79.4 bps/Hz [4]. Accordingly, 3GPP considers massive MIMO with up to 256 antennas for the first release of 5G [5]. Massive MIMO is both beneficial at conventional mobile network frequencies below 6 GHz, as well as at higher frequencies like the mmWave bands, both of which are being considered by 3GPP [5]. Besides these, other benefits of massive MIMO include extensive use of inexpensive low-power components, significant reduction of latency on the air interface, simplification of the Media Access Control (MAC) layer and robustness against interference and intentional jamming [1].

Although massive MIMO is agreed to being very beneficial in the access link, it induces substantial challenges on the fronthaul side, which have been discussed in D2.1 [2] and D2.2 [3] and are recaptured here.

In C-RAN networks, remote units (RUs) perform mostly only analogue RF processing, while the digital baseband processing is performed in central units (CUs). RUs and CUs are connected by a FH network. The currently dominant FH standard CPRI [7] defines, that a stream of time-domain I/Q samples is forwarded for each antenna element at the RU. With the current LTE implementation allowing for up to 8 antennas, this already requires a FH capacity of 24 Gbps (CPRI line rate option 10). In general, the required FH capacity can be calculated as

$$D_{\mathrm{CPRI}} = N_{\mathrm{A}} \cdot f_{\mathrm{s}} \cdot N_{\mathrm{Q}} \cdot 2 \cdot \gamma, \tag{2.1}$$

with N_{A} being the number of antenna elements, f_{s} being the sampling frequency, N_{Q} being the quantizer resolution, and γ being the transport overhead. Assuming the parameters given in Table 1, this would result in a FH capacity of 118 Gbps, which would incur a dramatic increase in FH CAPEX and OPEX. Accordingly, the concept of functional splits was introduced [8],[9] and was discussed for 5G-XHaul in D2.1 [2]. Functional splits define which part of the baseband processing is performed at the RU and which part at the CU. It thereby defines intermediate versions of the two extremes of either fully centralized C-RAN or the fully decentralized traditional RAN architecture. In general, the more processing is performed at the CU, the lower the requirements on the transport side are, as redundant signals can be removed. Figure 1 illustrates the different functional splits investigated within 5G-XHaul in comparison to CPRI.

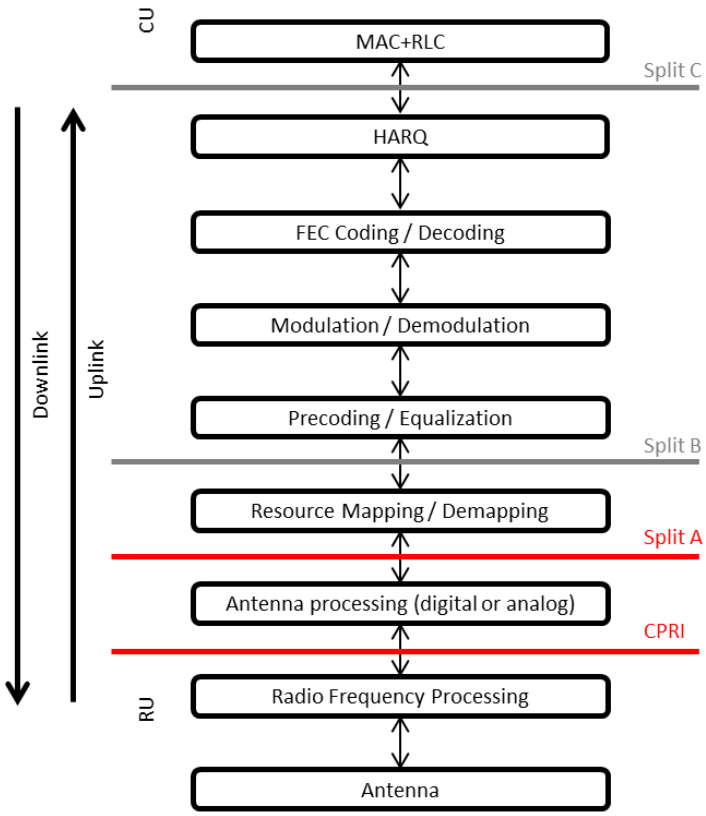

Figure 1: Functional splits.

Split A is specifically designed to mitigate the challenges arising from massive MIMO. By performing antenna processing at the RU, the number of stream transported over the FH no longer depends on the number of antenna elements but on the number of antenna ports, i.e. the required capacity is

$$D_A = N_{\mathrm{P}} \cdot f_{\mathrm{s}} \cdot N_{\mathrm{Q}} \cdot 2 \cdot \gamma, \tag{2.2}$$

with N_{P} being the number of antenna ports. The number of antenna ports can be chosen depending on the degree of spatial multiplexing desired. The required capacity for a traditional CPRI implementation and split A is compared in Figure 2. As can be seen, the FH capacity is reduced by factor 6. This illustrates how including baseband processing into the RU can significantly simplify the transport network while retaining the benefits of massive MIMO in the access link. 5G-XHaul hence considers this approach of partial L1 processing as a fundamental enabler for 5G transport networks supporting massive MIMO. As Split A addressed the massive MIMO challenge directly, it was selected for the development of the AAS, which will be described in the next section in detail.

It is important to note, while Split A is intended to mitigate the shortcomings of CPRI, the data streams forwarded can still be compliant with the CPRI frame format, as both splits require I/Q samples. The main difference is that additional MIMO processing is performed on top of the I/Q samples at the RU, which maps a small number of streams to a large number of antenna elements.

Table 1: Exemplary radio access parameters.

Parameter	Symbol	Value
Sampling Rate [MHz]	f_S	30.72
# Antenna elements	N_A	96
# Antenna ports	N_P	16
Overhead	γ	1.33
Quantizer resolution time domain	N_Q	15

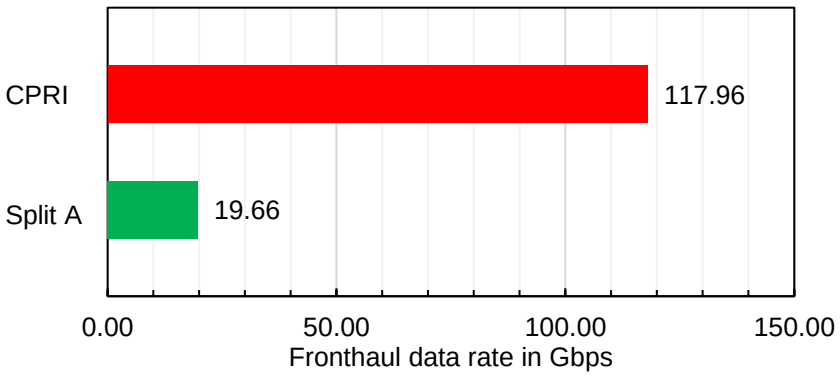

Figure 2: Comparison of required FH data rate for CPRI and Split A/advanced antenna system.

3 Advanced antenna system and baseband unit overview

3.1 Overall System Concept

In order to demonstrate the benefits of a “Split A” IQ interface as outlined above, 5G-XHaul develop prototypes for an AAS as well as BBU. The key components of the wireless system considered in 5G-XHaul are depicted in Figure 3. The system of interest for the purposes of this report consists of three parts: A baseband unit, which can be either run on dedicated hardware or run virtualized in a data centre, the advanced antenna system (AAS), and one or more user equipment (UE). The latter themselves include antennas, radios, and baseband implementation. The BBU and the AAS are connected through a transport segment that forwards I/Q samples to and from the AAS. In a life network, the BBU is further connected through the core network to an operator’s operations and maintenance centre. As indicated above, this report focusses on developments of a BBU, and AAS prototypes and the relation to the transport segment. For demonstration purposes a UE platform is outlined briefly. The individual hardware platforms are described in detail in the following sections.

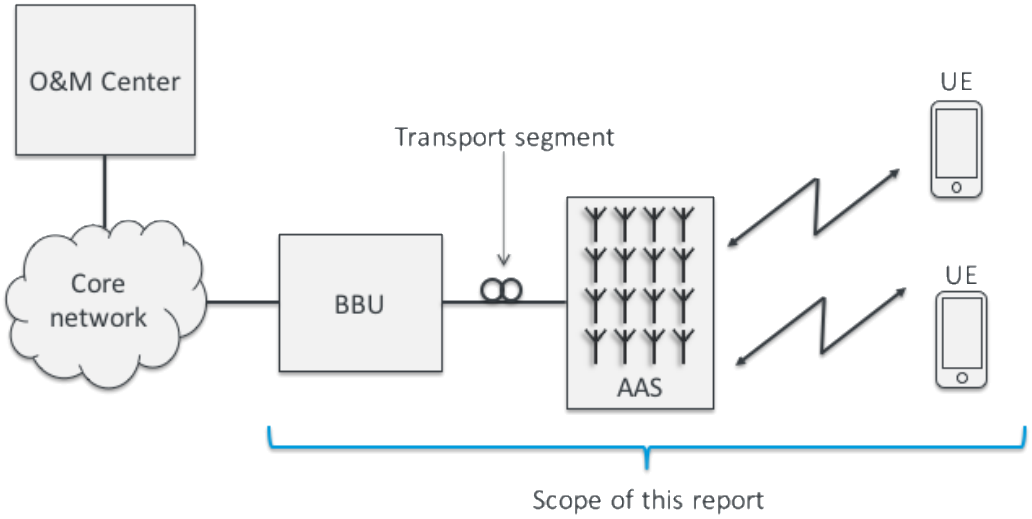

Figure 3: Cellular network system architecture

3.2 Baseband Unit and Receiver

Waveform

Massive MIMO is only one of many technological approaches to improve future radio access networks. Another approach is to utilize new waveforms, as proposed in [10]. These waveforms are intended to address various challenges such as low peak-to-average power ratio (PAPR), low out-of-band (OOB) emission, low bit-error-rate (BER), less complexity, asynchrony etc. Some of the main candidate waveforms include universal filter multi-carrier (UFMC), filter-bank–multicarrier (FBMC), GFDM, cyclic prefix orthogonal frequency division multiplexing (CP-OFDM), filtered OFDM (f-OFDM). While current pre-standardization for upcoming LTE releases focus on CP-OFDM [5], new waveforms might be still necessary for future releases or specific use cases. Hence, it is important to investigate the compatibility of new waveforms with other approaches like C-RAN and massive MIMO, to ensure that they are future-proof. Accordingly, Task 4.3.2 also studies the effect of new waveforms on future C-RAN architectures.

For this, GFDM [11] was selected as a representative future waveform. Its main benefit includes a low out-of-band radiation, which enables an easier operation in small bands (white spaces), and a higher number of occupied subcarriers due to the need for fewer guard carriers. Both will potentially lead to higher system

throughputs, as neighbouring bands will face less interference, and a higher effective bandwidth can be utilized. In addition, GFDM can be configured very flexibly, allowing for different subcarrier spacing, symbol durations, and block lengths, which could be adapted according to the use case, e.g., low latency or high throughput.

Figure 4 shows the spectrum of a GFDM waveform compared to conventional LTE, highlighting the much lower OOB radiation.

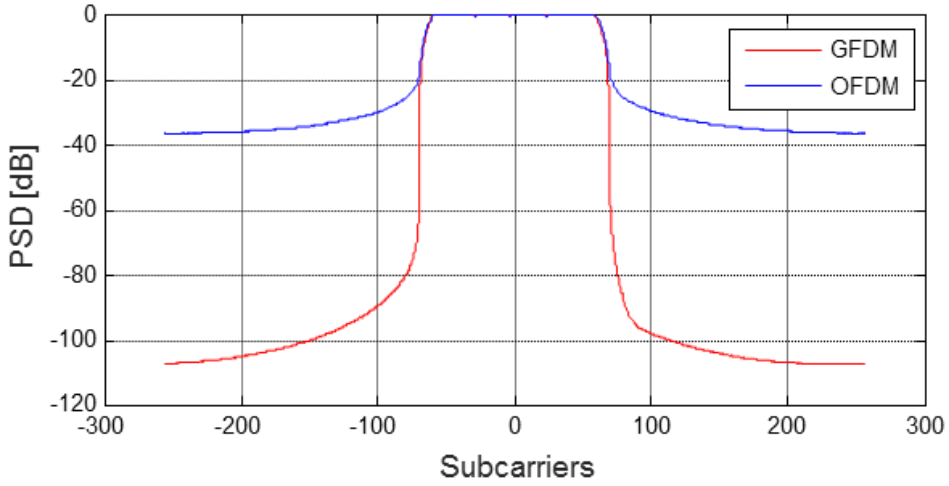

Figure 4: Power spectral density of GFDM vs. OFDM

The baseband unit implements transmit and receive functionality for such a GFDM waveform.

Baseband Architecture and Functionality

The baseband architecture is illustrated in Figure 5. The setup is composed of three parts:

- A MAC layer, implemented in NS3 on a Linux operating system.
- The upper PHY layer, implemented in Labview on a Linux real-time (RT) system.
- The lower PHY layer implemented on an FPGA.

For the RF part, the I/Q waveforms can be either be directly connected to an NI frontend, or connected to a CPRI FPGA card, where they can be fronthauled via fiber to the AAS and transmitted from there.

For reception, NI USRP systems together with a laptop can be used, implementing all functionalities from RF to the MAC layer.

The baseband supports basic transmission and reception functionalities, which are based on TLE Release 10, but modified to utilize a GFDM waveform. In detail, the functionality supported is:

- Uplink and downlink single link transmission with 20 MHz bandwidth in TDD and FDD mode.
- LTE compliant channel encoding and decoding.
- Data channels (PDSCH, PUSCH) and a simplified control channel (PDCCH).
- Reference symbols: CRS, UERS, PSS, SRS.
- RF impairment correction.
- Automatic gain control (AGC).
- Time and frequency synchronization.
- Cell-specific and UE-specific channel estimation.
- Channel equalization of data symbols.

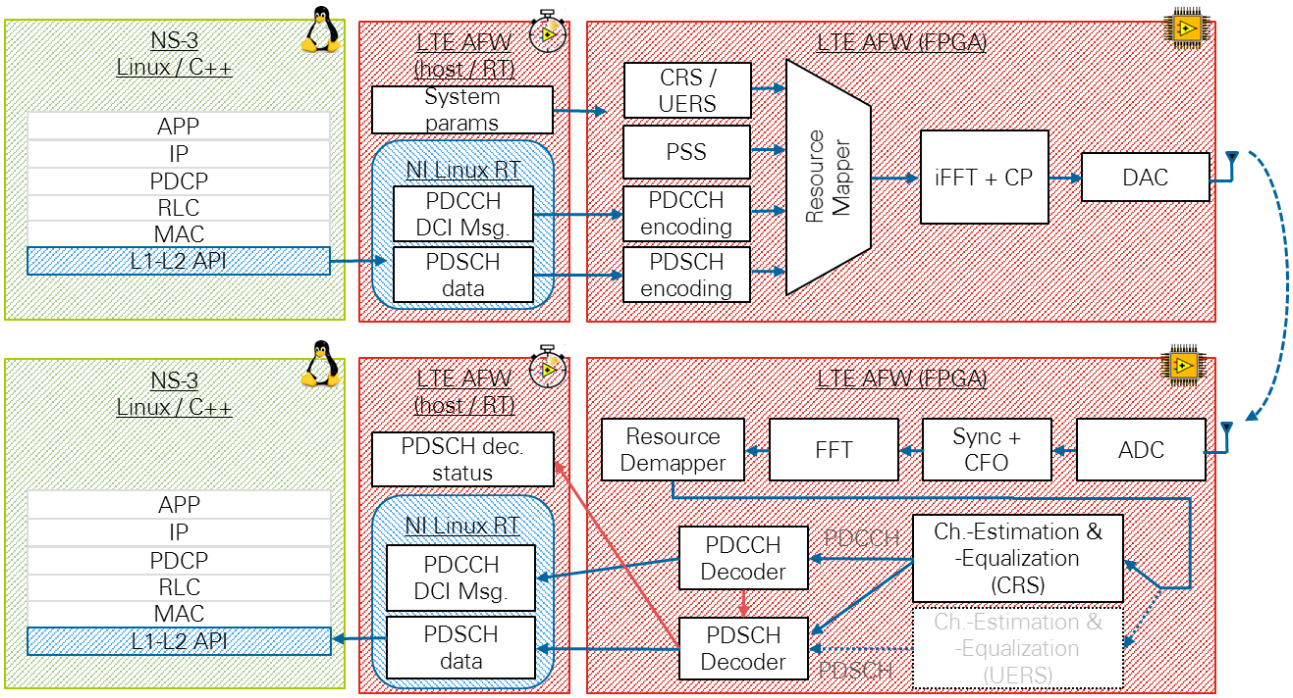

Figure 5: Baseband unit architecture.

3.3 Advanced Antenna System

3.3.1 AAS General Description and Characteristics

The goal of Airrays' innovation activity is to provide a proof of concept for an advanced antenna system with flexible digital beamforming capability. The target use case is network densification and provision of network capacity in urban and dense urban areas, which requires a medium range output power and a large number of independently steerable ports. Correspondingly, the AAS key features have been specified as follows:

- 12 x 4 cross-pol. Antennas.
- 96 transceivers.
- Built-in digital beamforming.
- Up to 16 steerable ports.
- up to 4 digital IQ interfaces (CPRI supported).
- Band 7, LTE FDD.
- Max RF output power of 12 W.

Band 7 is chosen since it is a global LTE band and currently being considered by most major European operators for LTE roll-outs. Band 7 thus provides the opportunity to trial an AAS prototype in an existing network.

In contrast to existing massive MIMO research platforms such as [4], the goal of Airrays' innovation activity in WP4 is provision of a platform that is prepared for immediate subsequent product development. This is in particular achieved by using highly integrated components for the transceivers, power amplifier (PA), filters, and digital processing platforms. The design approach allows for an AAS platform that goes beyond the state-of-the-art in the following aspects:

(1) Size: The 5G-XHaul prototype has a size of 900x265x100 mm, which corresponds to the form factor of a "typical" cellular antenna. In contrast, state of the art massive MIMO research platforms such as [4] and [5] feature much larger form factors, which is adequate for their purpose. Figure 6 compares the form factors of different AAS platforms.

5G-XHaul AAS prototype front view

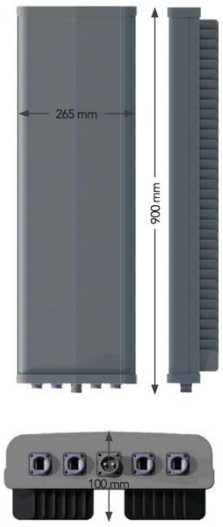

5G-XHaul AAS prototype dimensioning

AAS research platform front view [5]

Figure 6: Comparison of AAS platforms. Left and middle: 5G-XHaul prototype with 96 transceivers. Right: State of the art research platform from [5] with 128 transceivers.

(2) Power consumption: High integration allows for much lower energy consumption than is needed in a research platform. This is due to lower power per component but also due to lower losses on the interconnects where virtually no cables are required. Even though a complete evaluatoin of the power consumption is not available yet, an average conumption of about 500 W is expected.

(3) Last but not least, existing economies of scale for the key components, in particular transceiver ICs, PAs, filters, and compute platforms, enable competitive pricing per radio unit after the commercialization phase.

Table 2 summarizes key electrical characteristics of the AAS prototype. Table 3 summarizes key characteristics related to the digital interface, features antenna performance (i.e. antenna gain) and other supported features. These parameters are derived from a use case and requirements study reported in [15].

Table 2: AAS electrical characteristics.

AAS electrical characteristics	
Frequency Band	Band 7 UL: 2500-2570MHz DL 2620-2690MHz
Polarization	±45°
Vertical Beamwidth	9.3° ± 1.0°
Horizontal Beamwidth	25°
Horizontal Beamwidth tolerance	± 3°
Beamwidths	Variable both horizontal and vertical
Inter / Intraband Isolation	>28dB
Front to Back Ratio 180°± 30°	>25dB
Intermodulation: 3rd order for 2 x 10W carriers	>153dBc

Table 3: AAS Digital I/O and performance characteristics.

AAS Digital characteristics	
RF Output	12W (with Sidelobe Suppression < 10W)
Built-in Beamformer	Option to map antenna carrier to beam
Number of supported antenna carriers	16
Number of simulatenous Tx beams	16 (8 for +45°, 8 for -45°)
Number of simulatenous Rx beams	16 (8 for +45°, 8 for -45°)
Separate Tx and Rx beams	supported
Precomputed grid of beams	supported
Individual power settings per beam	supported
Freely programmable beamforming vectors	supported: phase and amplitude for each antenna element can be set
Carrier aggregation	contiguous CA up to 40 MHz
Different beam patterns for up- and downlink	supported
Gain (max)	21.6 dBi
EIRP (max)	61.6 dBm
Electrical Tilt per beam (Vertical)	-45° to 45°
Electrical Tilt per beam (Horizontal)	-30° to 30°

3.3.2 AAS Principal Architecture

Principal Functional Blocks

The high level architecture of Airrays 5G-XHaul radio unit is depicted in Figure 7. The overall unit is composed of three main functional layers: a digital processing layer, an RF layer, and a radiating layer.

The **radiating layer** includes the dual polarized antenna elements including SMP connectors through which RF signals are fed into the elements. This layer is responsible for radiating RF signals with minimal mutual coupling.

The **RF layer** is comprised of 96 transceivers and RF front-ends. Each transceiver includes a dedicated ADC and DAC, up- and down converters, and digital filters. Besides the duplex filter, the front-ends feature drivers, transmit filter, and power amplifier in the transmit path as well as receive filter and LNA in the receive branch.

The **digital processing layer** comprises the interface to the baseband, control functions, as well as key functional blocks such as array calibration and beam processing in transmit and receive paths. Beam processing for the downlink comprises the complex weighting and mapping of digital IQ streams received from the BBU onto all 96 transceivers. In the uplink digital IQ streams are received from all 96 transceivers and combined into up to 16 streams corresponding to 16 antenna ports. A beam pattern data base is provided to store precomputed radiation characteristics in form of their complex weights. Array calibration comprises all processing necessary to ensure strict phase alignment of all transceivers as well as alignment of individual sampling times.

Note that the inclusion of a digital processing layer and in particular of beam processing in the AAS enables realization of the functional Split A. For massive MIMO radio units a significant reduction of the data rate requirements on the transport segment compared to a classical fronthaul CPRI split is a necessary prerequisite for commercialization of this 5G technology.

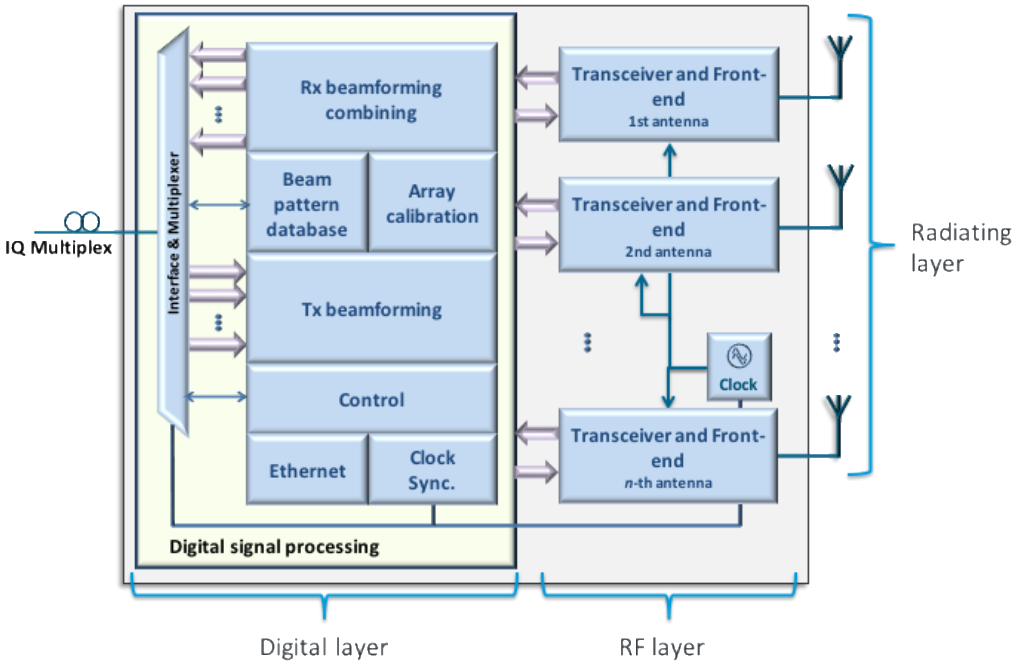

Figure 7: Functional block diagram of Airrays radio unit.

Modular Hardware Architecture

The AAS hardware concept adopts a modular design such that each radio unit is composed of a number of modules, called radio subunits (RSUs), which are identical in construction. Each RSU features 8 complete transmit and receive chains in a 2x2 cross-polarized configuration as well as its own digital processing platform. A single interface module, called the interface subunit (ISU), provides the interface to the BBU as well as central control and calibration functionality. Figure 8 shows the current radio unit prototype consisting of 12 RSUs and a single ISU.

Note, that this modular approach provides significant advantages over a commonly used centralized design:

- It allows re-use of a single hardware RSU design to realize radio units of different sizes and shapes.
- By using distributed processing on each module, there is no single major heat source and heat can be dissipated more effectively.
- Component cost of digital processing decreases in a distributed compared to a centralized architecture.
- RF tests can be performed per module, which are much easier to handle than complete radio units.

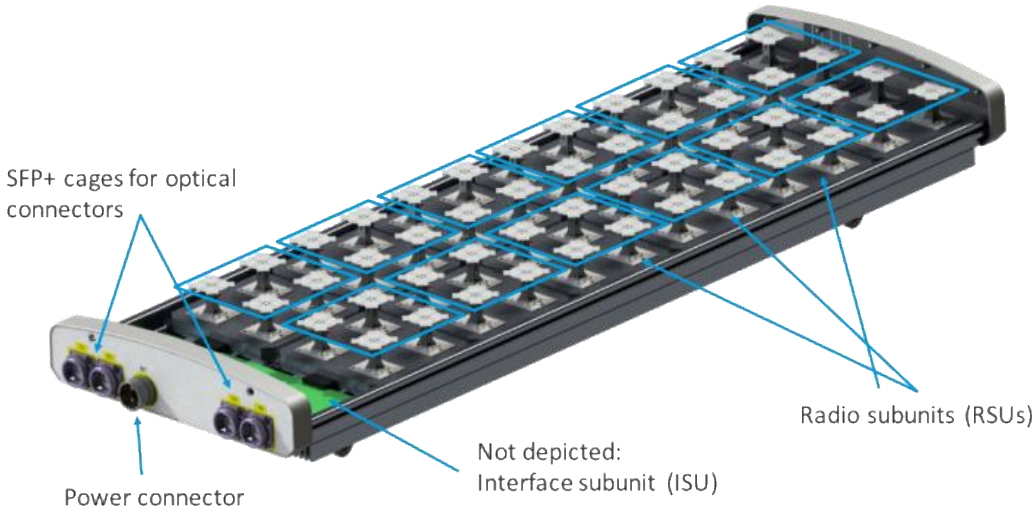

Figure 8: The 5G-XHaul AAS prototype consisting of twelve RSUs and one ISU.

The three principal layers of the architecture described in the previous paragraph are mapped onto each RSU, which is illustrated in Figure 9. The radiating layer is realized by 4 cross-polarized antenna elements including antenna cages to reduce cross-coupling. Both RF layer and digital layer are realized in hardware on separate boards, with high speed connectors between them.

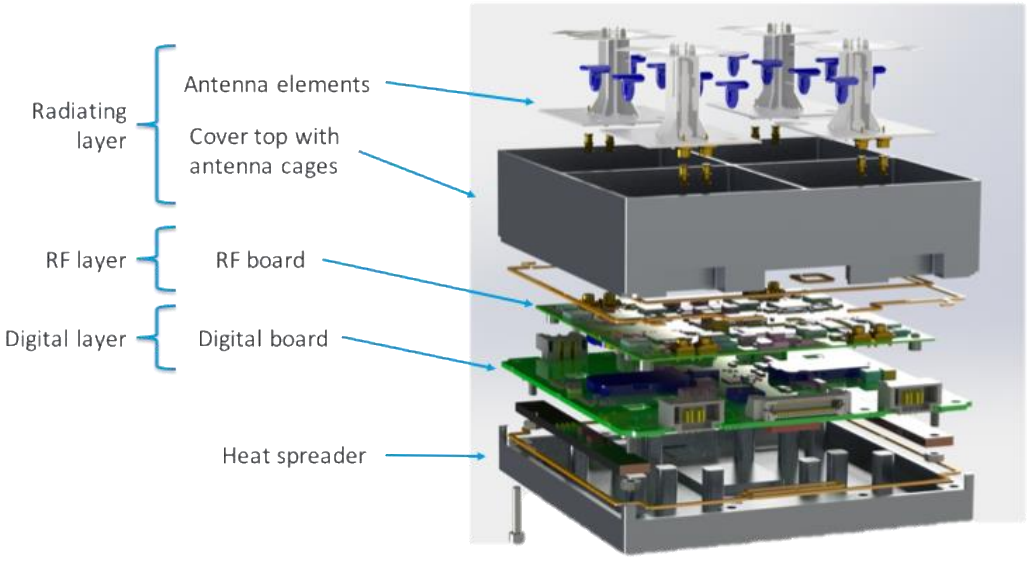

Figure 9: RSU hardware design.

4 Initial test results and development status

4.1 Initial Tests of the Baseband Unit

Test Concept

To verify that GFDM can be utilized in a C-RAN setting as intended for the AAS, initial tests were performed. As the main benefit of the GFDM waveform is its low OOB, it was necessary to investigate whether the low OOB can be maintained after FH transmission and RF processing. The two main effects studied for this are the quantizer resolution and PA non-linearities.

GFDM has less OOB emission compared to OFDM; however, this gain is in digital domain. The waveform generated at the Remote Unit (RU) is in digital domain which is converted to analogue domain by digital to analogue converter (DAC) at RU. As can be seen from Eq. (2.2), the quantizer resolution N_Q scales the capacity required on the FH. As the samples are transported on the FH with a limited resolution, they need to be quantized, which adds quantization noise. Figure 10 and Figure 11 illustrate simulated GFDM and OFDM waveforms quantized with different resolutions, N_Q.

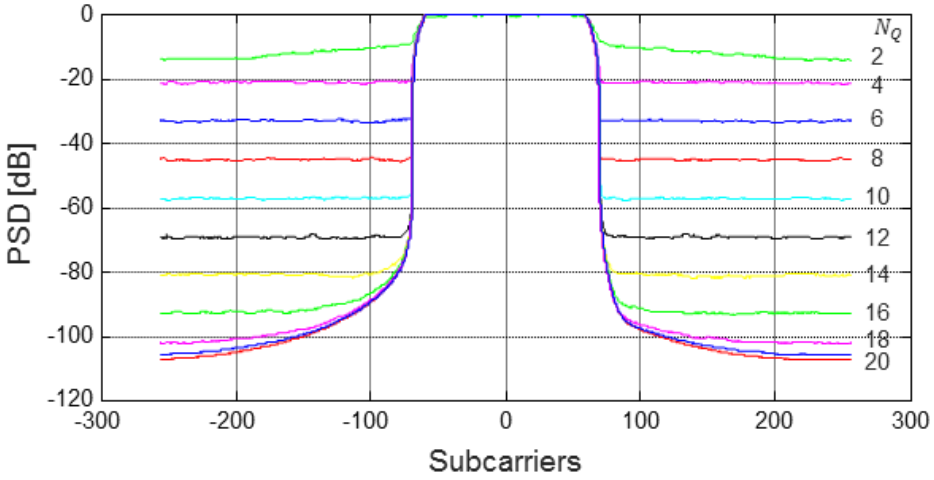

Figure 10: Power spectral density of GFDM for different quantizer resolutions.

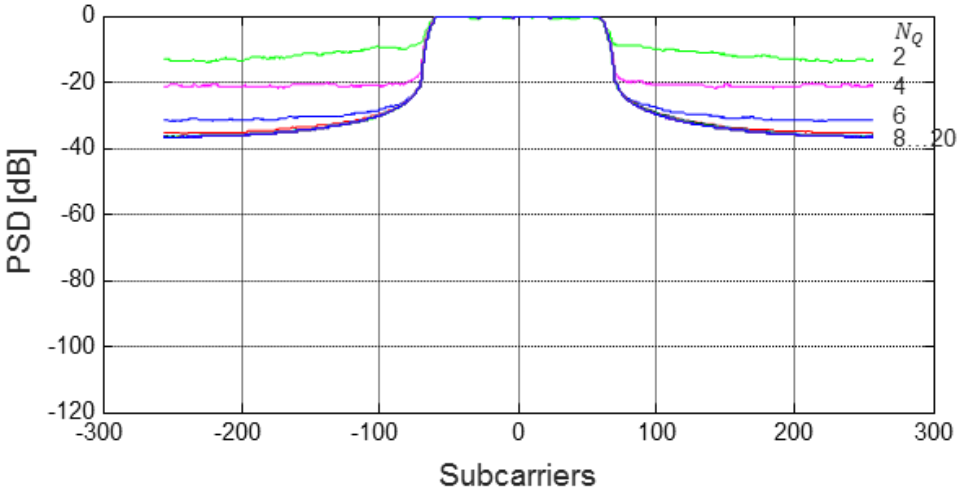

Figure 11: Power spectral density of OFDM for different quantizer resolutions.

As can be seen, the quantization adds white noise, which has a severe impact on the OOB power spectral density (PSD). For each additional bit, the signal-to-quantization-noise ratio (SQNR) improves approximately by 6 dB. This can be easily seen for lower bits such as 2 bit, 4 bit, 6 bit and 8 bit. Only once the resolution is chosen high enough, the waveform becomes the limiting factor of the PSD. Up to 8 bits are necessary for LTE, and up to 20 bits for GFDM to achieve full PSD reduction.

However, the PSD is not the deciding metric, as most interfering power is concentrated in the frequencies at the bands edge. The overall OOB radiation is defined [11] as the ratio of amount of amount of energy emitted to the out of band region to the amount of energy within the allocated bandwidth, which is illustrated in Figure 12.

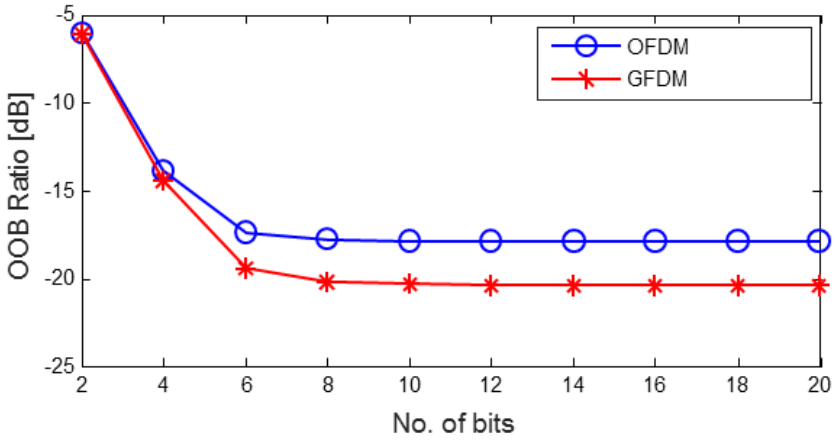

Figure 12: OOB ratio for GFDM and OFDM.

As can be seen, both GFDM and OFDM require resolutions of 8-10 bit to achieve full OOB reduction, which is less than the commonly used resolution of 15 bits[1] in LTE. In total, GFDM showing the overall better performance. As these results are based on simulations, it is necessary to verify the observations in the demonstrator setup. A second factor impacting the OOB performance is the PA. As a PA only has a limited dynamic range, it will add non-linear distortion if operated with a high gain, which also reduces the OOB. While this problem is common both for C-RAN and conventional RANs, it is necessary to verify that the proposed demonstrator can operate with the GFDM waveform. Accordingly, initial measurements were performed, which are described next.

Measurement Setup

In order to perform measurement, first I/Q samples of GFDM and OFDM waveforms were quantized according to the desired resolution. Then, they were forwarded to a NI 5791 transceiver (TRX) module and transmitted via cable to a spectrum analyser shown in Figure 13, and out-of-band radiation was measured. Next, a PA is connected between the TRX and spectrum analyser. Output of TRX was first fed to PA and then output of power amplifier is fed to the spectrum analyser via a 60 dB attenuator. The power amplifier operates at the TX frequency of 2.19 GHz and it provides maximum 36 dB gain and 50 dBm (100 mW) output power. In order to sweep different gains of the amplifier, a real time application was used to set gain of the amplifier. The OOB measurement was repeated for 50 iterations and average values were noted to have more accurate results, as the measurements are impacted by thermal noise, signal clipping before transmission, and signal distortion on the utilized cables, connectors, and attenuators. Table 4 shows the measurement parameters used for the measurement set up OOB analysis of GFDM and OFDM. As input to the PA was not sufficient to drive the amplifier into nonlinear region, two amplifiers were connected in cascade such that amplified signal from the first amplifier is fed to the input of the second.

[1] Note that the quantizer resolution does not only depend on the OOB but also e.g. on the precision required for LLR calculation. Accordingly, a higher resolution is chosen in LTE than would be required from the OOB point of view.

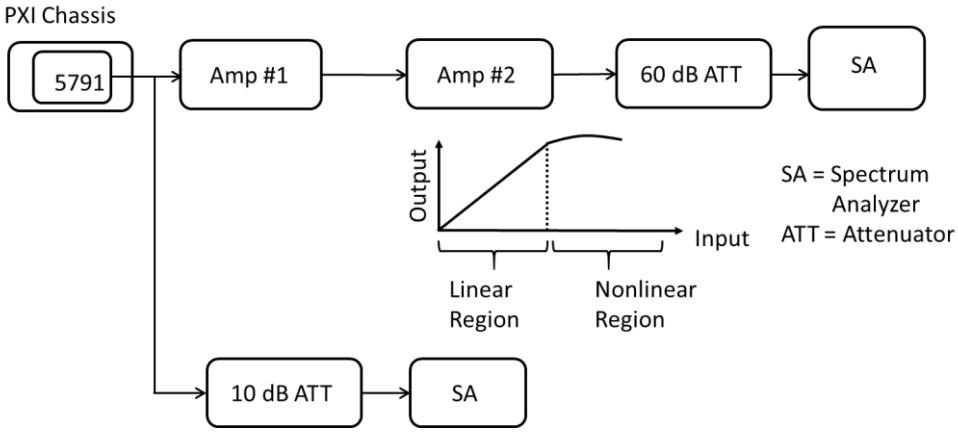

Figure 13: Baseband unit measurement setup.

Table 4: Baseband unit measurement parameters.

Parameter	Value
Carrier frequency	2.19 GHz
Sampling frequency	7.68 MHz
FFT size	512
No. of occupied subcarriers	64
No. of subsymbols	14
Subcarrier spacing	15 kHz
GFDM roll-off factor	0.1
GFDM transmit filter	Raised Cosine
Modulation	4-QAM

The Impact of Quantization

Figure 14 shows OOB ratio for different number of bits for GFDM and OFDM. In this case, OOB ratio was measured by directly transmitting the waveforms to the spectrum analyzer without connecting the power amplifier. As seen from the figure, OOB ratio is much higher at lower bits such as 2 bits and 4 bits since quantization noise for lower bits is much higher. This ratio decreases at higher bits. Moreover, it is also evident from the figure that GFDM still have better OOB emission though the differences between OOB of GFDM and OFDM is subtle. Comparing the measurement in Figure 14 with the simulation in Figure 12, we see that the OOB ratio in case of measurement is less than that of simulation figure. This difference is more pronounced in GFDM waveform and is caused possibly due to RF losses.

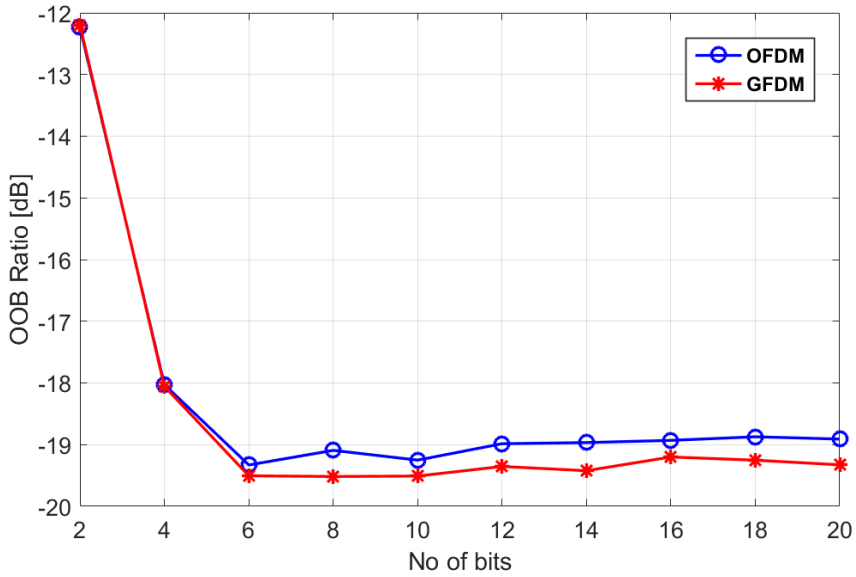

Figure 14: Measured OOB ratio vs. quantizer resolution.

Impact of Power Amplifier

The OOB ratio does not change much at higher bits. Hence, a fixed number of bits were selected (in this case 12 bits) and OOB ratio is plotted for different gains of the first amplifier as shown in Figure 15. Furthermore, the gain of the second amplifier was fixed at 30 dB and gains of first amplifier were varied such that we get both linear and nonlinear regions of the second amplifier. It is clear from the Figure that the OOB ratio is nearly constant in the linear range from 0 to 6 dB of the amplifier gain. As the gain increases further, amplifier reaches nonlinear region and OOB ratio increases abruptly. An amplifier is said to be in nonlinear region when the output of amplifier does not follow the increase in input. In the linear region, GFDM has about 1 dB less OOB emission compared to OFDM. In the nonlinear region, distortion is dominating and there is very subtle difference between GFDM and OFDM.

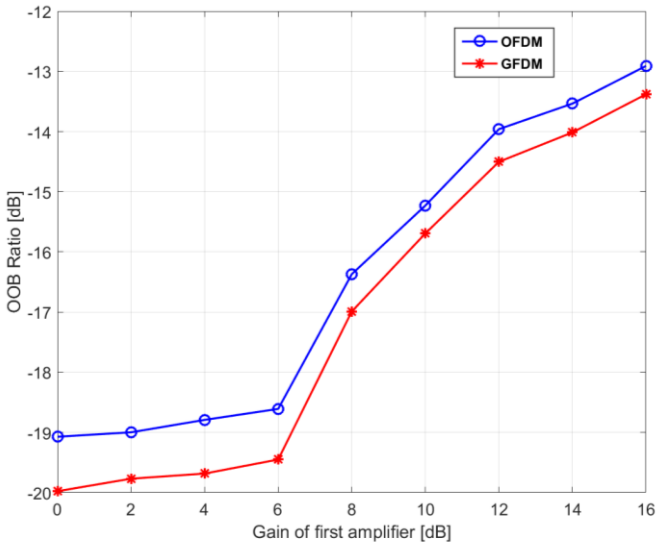

Figure 15: Measured OOB ratio vs. pre-amplifier gain, which determines the operating point (linear range or non-linear range).

4.2 Initial Tests of the Advanced Antenna System

The following sections describes the status of the RU development and an initial set of measurements that document the progress of development. In these measurements, the focus is on the RF performance in both, transmit and receive direction, which is reported in Section 4.2.1.

As outlined in Section 3.3.2, the AAS is composed of 12 identical RSUs. As a necessary step to bring up such a modular design, the digital high-speed interfaces between RSUs and towards the distributed transceiver ICs are tested, which is reported in a separate section below.

Finally, also results of the AAS transmitting GFDM waveform provided by TUD are shown to demonstrate the capabilities of the AAS to operate with 5G-related waveforms other than OFDM.

All RF tests reported here are performed on a single transmit or receive chain. In the coming phase of the project, the available RSUs will be integrated to a field trial ready beamforming RU which is to be trial in spring 2017. In Section 5.2, we will give an outlook of the field trials planned.

4.2.1 RF Measurements

The RSU as shown in Figure 9 is available and being tested with respect to RF performance and all major interfaces. While some measurements are done in configurations of multiple connected modules, the RF performance is measured for single antenna ports for both RX and TX direction. Conducted measurements are performed at individual antenna ports. The transceiver and RF frontend in the system context is depicted in Figure 16.

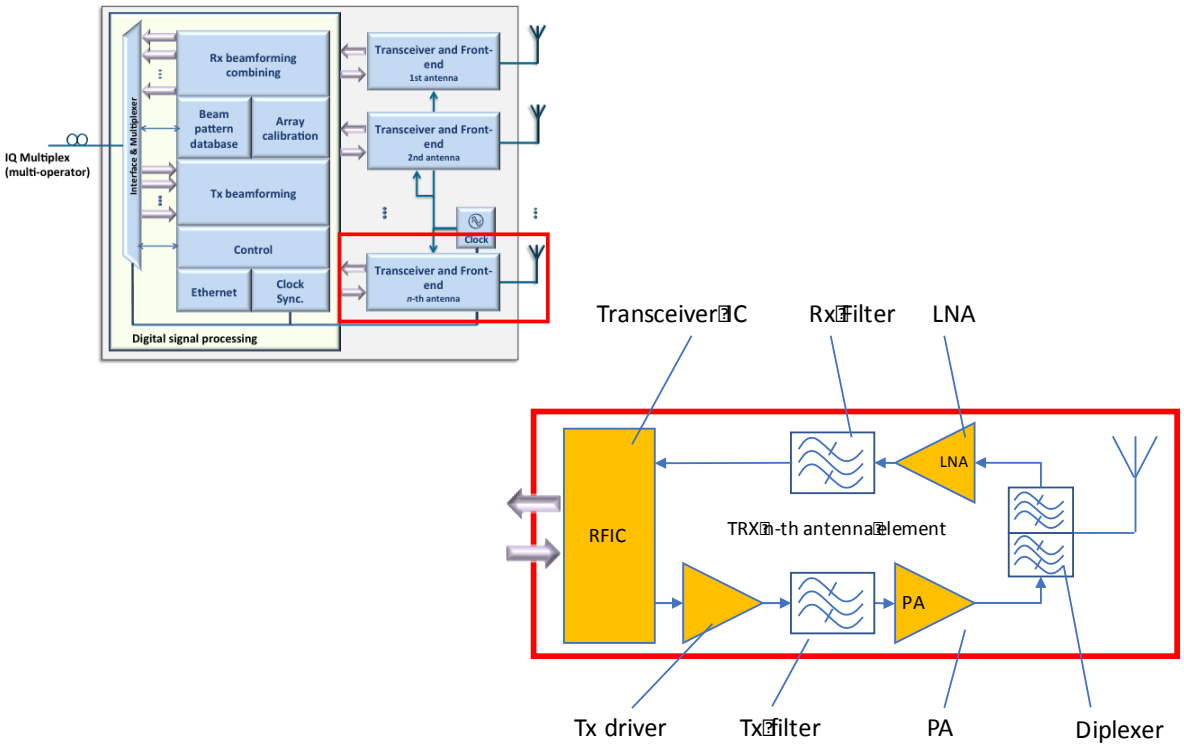

Figure 16: RSU with 8 antenna ports and detailed block diagram of the transceiver chain.

Test setup

The complete test setup for RF measurements is shown in Figure 17. The setup is configurable and is, therefore, used for downlink as well as uplink measurements. The SP8T switch matrix is a configurable adapter to

connect any of the 8 antenna outputs of the RSU and to the signal analyser (for downlink) or the signal generator (for uplink measurements).

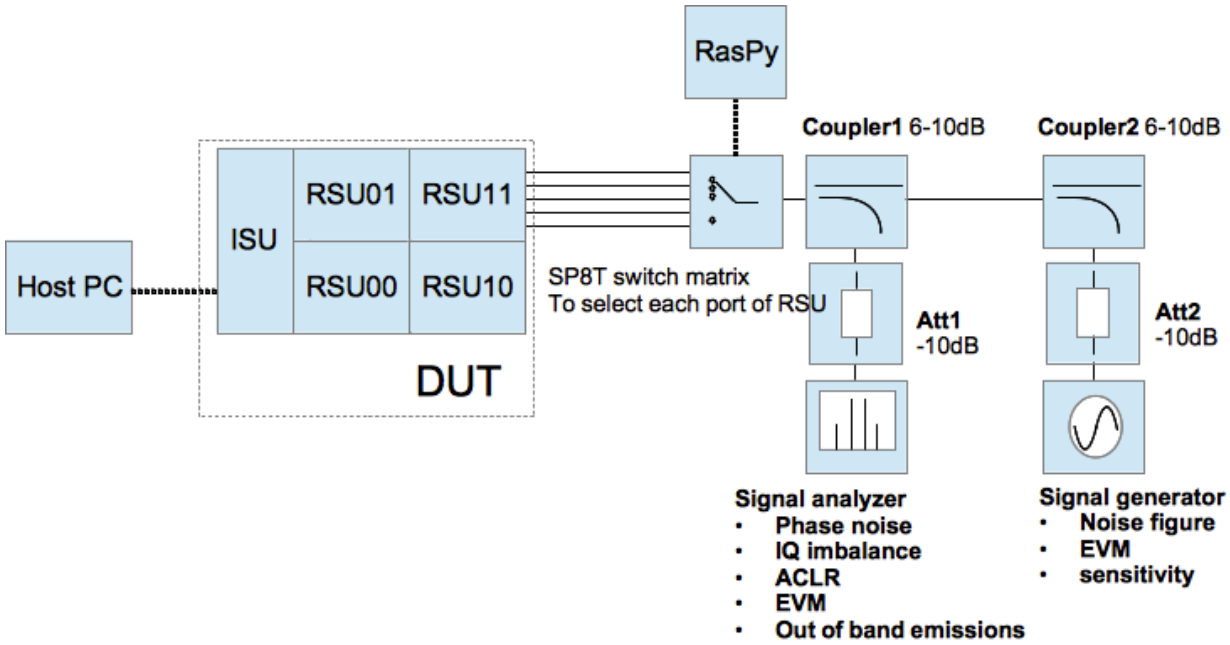

Figure 17: Configurable setup for uplink and downlink measurements.

Most of the measurements reported here are done in a configuration with the DUT being a single RSU connected to a Xilinx KC705 evaluation board is depicted in Figure 18. The KC705 also contains a waveform memory used to sample and play BBU signals. The BAB-BB is an adaptor board which is required to connect the RSU to the KC705. It is not part of the final prototype antenna.

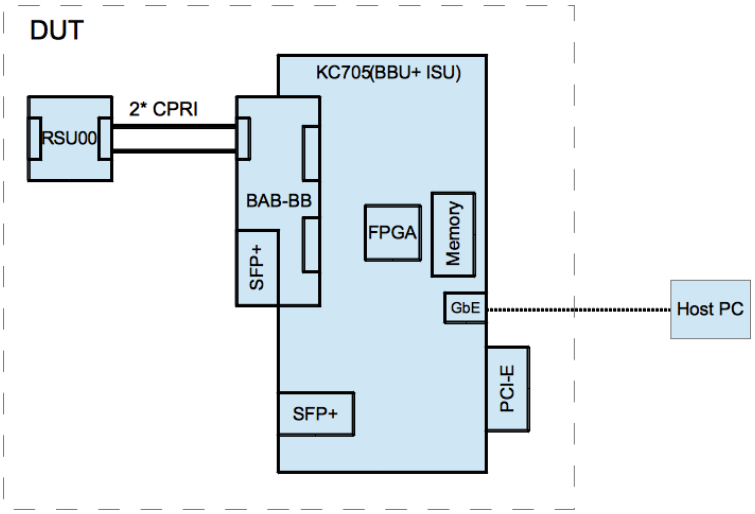

Figure 18: DUT as used in the measurements reported below (if nothing else is stated).

Clock and Phase Stability

A fundamental RF measure is phase noise (PN) of the local oscillator. For the single antenna ports, we target an integrated phase noise below 1°. Figure 19 shows a typical PN measurement. The measured value is

0.394° which is well below the target and, therefore, leaves margin for temperature and power supply variations. The measurement shown in Figure 19 is performed at a single antenna port and is representative of the measurements performed at other ports.

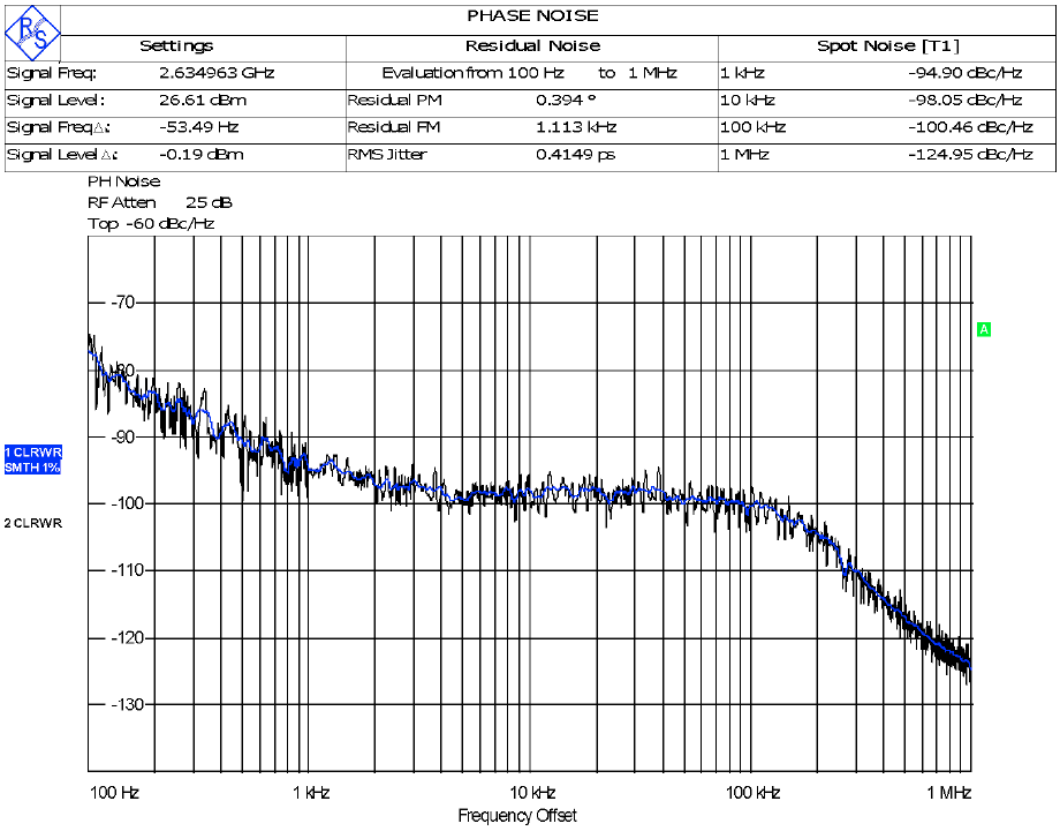

Figure 19: Phase noise of the local oscillator of a single TX port.

RF Calibration

The transceiver signal chain is depicted in Figure 20. To achieve the required signal quality, the transceiver needs to be calibrated for optimum ACLR as well as EVM at a given carrier frequency, bandwidth, and RF output power, which define the operating point. Optimum parameter settings of the transceiver IC (TRX-IC) to achieve minimum phase noise, error rates of the digital interface, etc. were determined in a bring-up phase through parameter sweeps. Relevant parameters include, among others, tunable capacities, resistor values in filter banks, and gain settings, all specific to the transceiver IC implementation.

In addition, parameters for IQ imbalance and DC offset compensation are automatically optimized through firmware algorithms for each operating point and are tracked over time using these calibration algorithms. Effects that need to be compensated for include IQ imbalance and DC offset. Using appropriate algorithms, image rejection of > 50 dB was achieved for TX and RX.

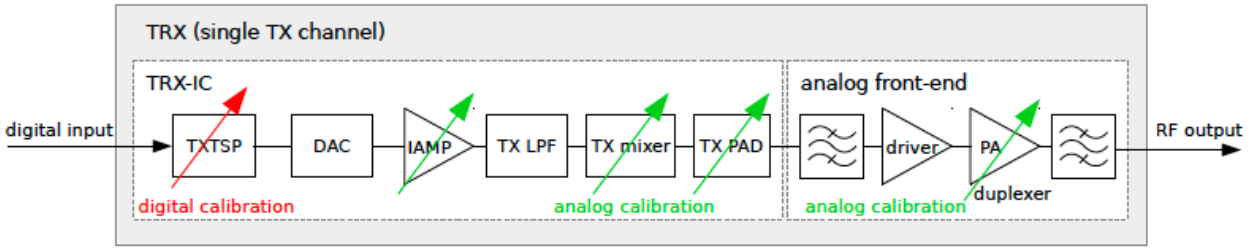

Figure 20: Simplified block diagram showing a single channel of transceiver path (single channel).

RF Measurements of the Receiver Chain

The radio unit has an RF bandwidth of 40 MHz to support continuous carrier aggregation. Each transceiver is connected to a processing unit (realized as an FPGA on the RSU). For the measurements shown in this section, the received samples are captured in a memory on the FPGA and analyzed offline for the relevant RX parameters. The RX spectrum measured in a conducted configuration is shown in Figure 21. The measured signal has an SNR of about 30 dB.

While the receiver chain is still subject to future optimization, this measurement confirms that the performance of the receive chain meets expectations.

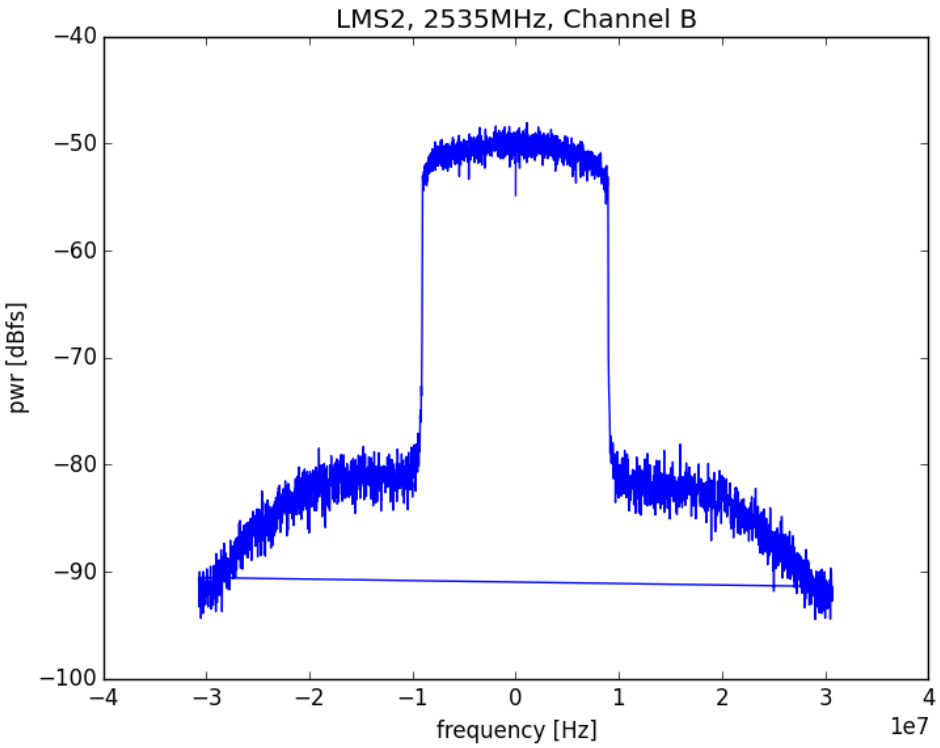

Figure 21: RX spectrum measured in a conducted configuration.

Another important parameter of the RX performance is noise figure of the RF frontend. Figure 22 shows noise figure measured for different carrier frequencies in LTE band 7.

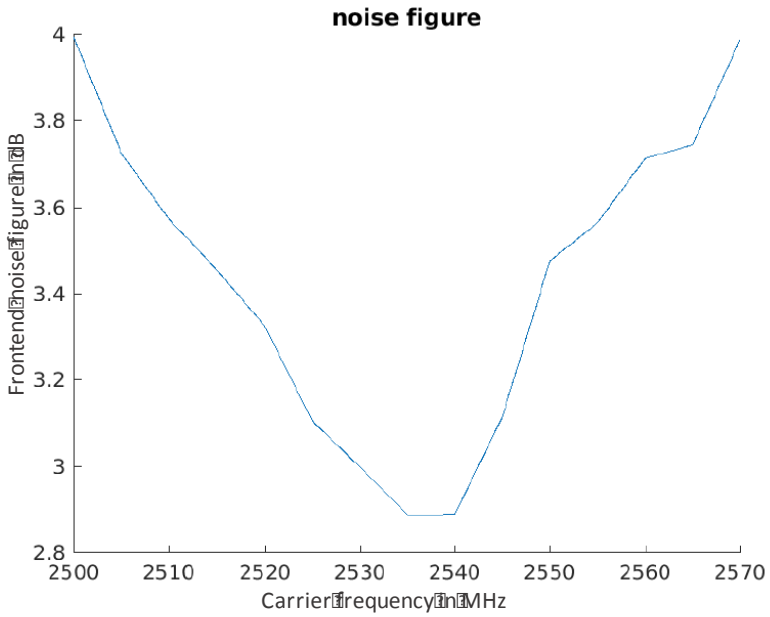

Figure 22: Measured frontend noise figure.

The measurement shows performance as expected with a noise figure of 4 dB at the band edges. The noise figure at the band edges is higher because the matching network is optimized for the band center and because the duplex filter attenuation is higher at the band edges. The duplex filter is a BAW filter, because the filter should be as small and cheap as possible. On the downside, this duplex filter has a pass band attenuation of about 2-3 dB. It is, therefore, the greatest impact to the noise figure.

A noise figure of 4 dB is common in state of the art remote radio heads if the connection between RRH and passive antenna is also considered. Therefore, the noise figure performance measured here meets expectations.

RF Measurements of the Transmit Chain

The ACLR is one of the most important parameters for undesired spectral emissions. 3GPP TS36.104 subclause 6.6.2 requires ACLR to be below -45 dB. As described in Section 4.1, OOB spectral emissions increase with output power because of PA saturation. The target is to fulfil 3GPP requirements at an output power of 21 dBm for each port which corresponds to total radiated power of 12 W. The measured ACLR is shown in Figure 23. In the current proof-of-concept phase the target is not achieved throughout the complete band, especially, considering that some headroom is required to account for process and temperature variability. However, the matching of the current design will be subject to further optimizations which are expected to solve the issue.

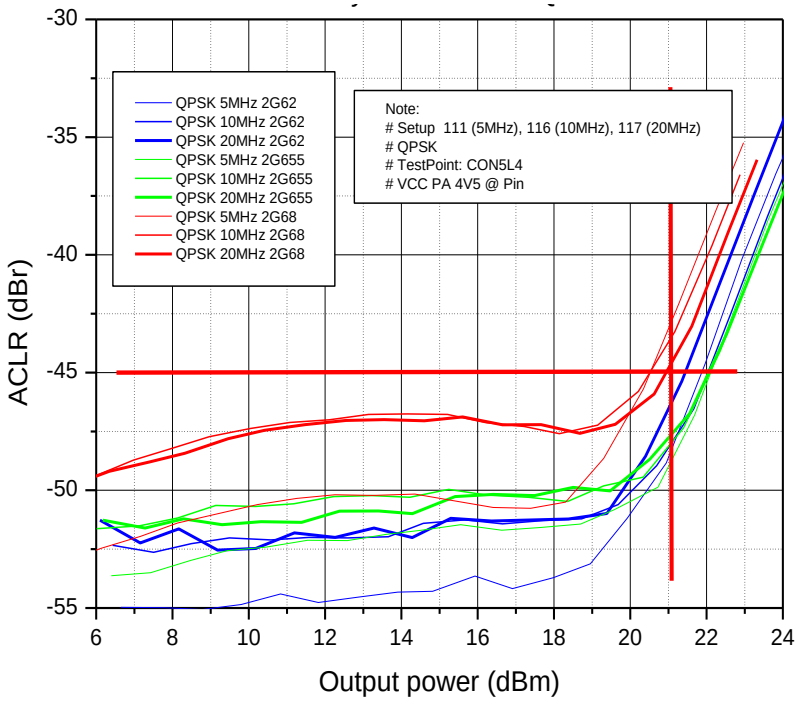

Figure 23: ACLR for different LTE signal bandwidths.

Another important parameter which shows RF performance is EVM as specified in TS36.104 sub-clause 6.5.2. Figure 24 shows the measured EVM for a 5 MHz LTE signal transmitting 64 QAM. An EVM of < 2.5% at the target output power is very good and leaves sufficient margin for temperature or device dependent variations even if an internal target of 3% is considered. An EVM of 3% is a typical mobile network operator requirement.

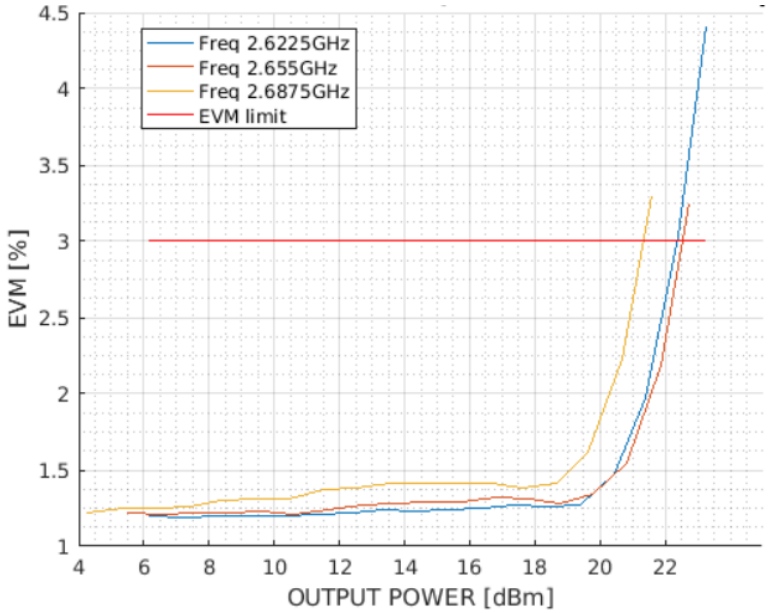

Figure 24: EVM for different carrier frequencies [LTE 5 MHz, 64 QAM].

RF Measurements using a GFDM Waveform

GFDM was already introduced in Section 3.2. In order to verify that the Airrays AAS is also suitable for transmission of 5G waveforms, an initial test was performed. In this test, the signal was streamed from the KC705 to the RSU and transmitted from a single antenna port, which is the setup shown Figure 18. The measured TX spectrum is shown in Figure 25.

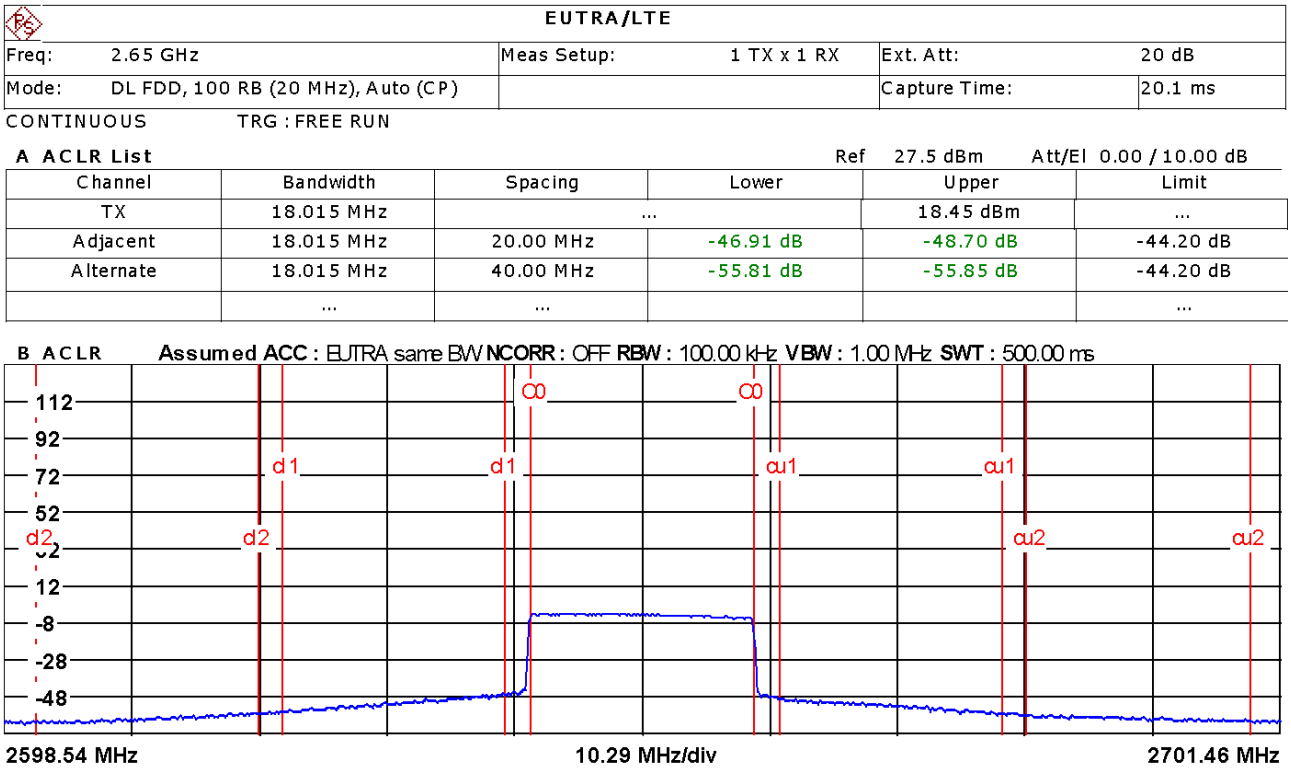

Figure 25: Spectrum of a transmitted GFDM signal and ACLR measurement.

Comparing this result to the ACLR measured for LTE signal shown in Figure 23, the result is in the same order. An important difference, however, is that the LTE signal was filtered in the digital BB for reduced OOB distortion. This filtering is not required for GFDM which is significant, especially considering low bandwidth channels which have a very short cyclic prefix which does not allow for much digital filtering.

4.2.2 Inter-RSU High-Speed Digital Interface

The 5G-XHaul AAS prototype follows a modular design. Multiple RSUs are connected through a digital high speed interface of 2 x 10 Gbps. The connection is electrical, realized through the pins of the board to board connectors.

A setup with two connected boards is shown in **Figure 26**. The high-speed links were brought up with the various loop back modes of the high-speed transmitters of the FPGAs, internal test signals as well as test signals generated on the base KC705. Multiple end-to-end tests of the various high speed links were run over a period of two hours and tested with zero bit errors.

Note that, the RSU was connected to a Xilinx KC705 evaluation board (through an adaptor board) which, currently, is the ISU and a BS emulator in one device. A prototype of the actual ISU is on the way and will be available for integration early 2017. In the field trial setup described in Section 5.2, the KC705 will still be used as a BS emulator.

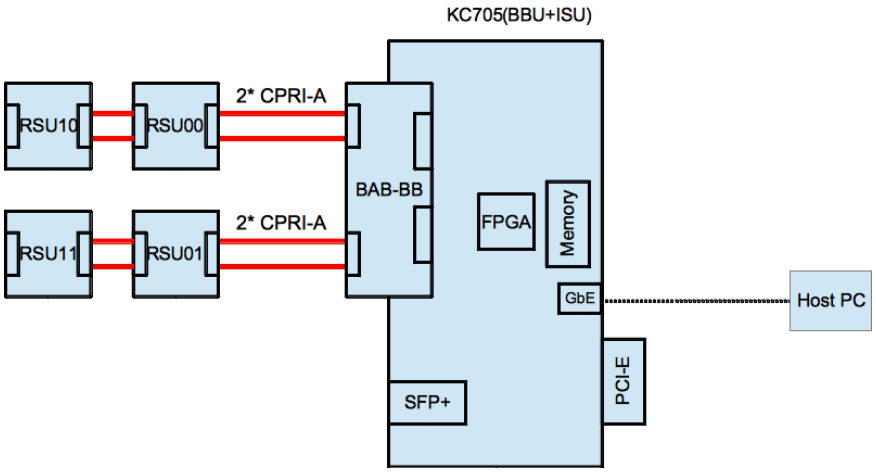

Figure 26: Picture of four RSUs that are connected in two daisy chains to the KC705. The high-speed links are marked in red.

5 Summary and Outlook

5.1 Summary

This report provides an overview of the hardware concepts of two 5G-XHaul hardware platforms: (1) A 5G BBU which is used to develop and test algorithms and concepts for new waveforms for radio access. (2) A massive MIMO AAS which features 96 transceivers, digital L1 processing and which implements a functional split that reduces the fronthaul data requirements by factor of six to twelve for eight and sixteen virtual ports used at the AAS, respectively. Initial tests are performed on both platforms. These include OOB performance of the GFDM waveform generated by the BBU and RF performance such as ACLR, EVM of the AAS. The performance results of both platforms meet regulatory requirements as well as expectations. The goal of these activities is demonstration of key enabling technologies for flexible and re-configurable transport networks and 5G.

5.2 Outlook: Field Trials

The initial tests reported in the previous section are the first step towards a trial-ready AAS. All measurements reported here are performed on a single RSU except for the tests of the high speed interface. After full integration of 12 modules into a complete radio unit, an RF characterization of the complete AAS will be performed after which the beamforming capabilities of the AAS can be demonstrated in the field.

At this point, two separate trials are considered:

- **Trial 1** will demonstrate the beamforming capabilities of the AAS with several parallel links in the radio access. This trial is planned to take place in the NITOS testbed in University of Thessaly (**UTH**).
- **Trial 2** will demonstrate the interworking of the AAS with 5G-XHaul dense wavelength division multiplexing (DWDM) transport technology. This trial is planned to take place in the **BIO** testbed in Bristol.

Both field trials are part of the activities performed in 5G-XHaul WP5. We provide a brief outlook of both trials below.

Trial1: Beamforming in the Radio Access

The field trial setup is shown in Figure 27. The trial shall show several GFDM streams being transmitted through several parallel beams of the same AAS. In order to drive the AAS, the trial setup uses a base station emulator implemented on a KC705 FPGA board. The Base station emulator connects to the ISU of the AAS through an optical CPRI interface.

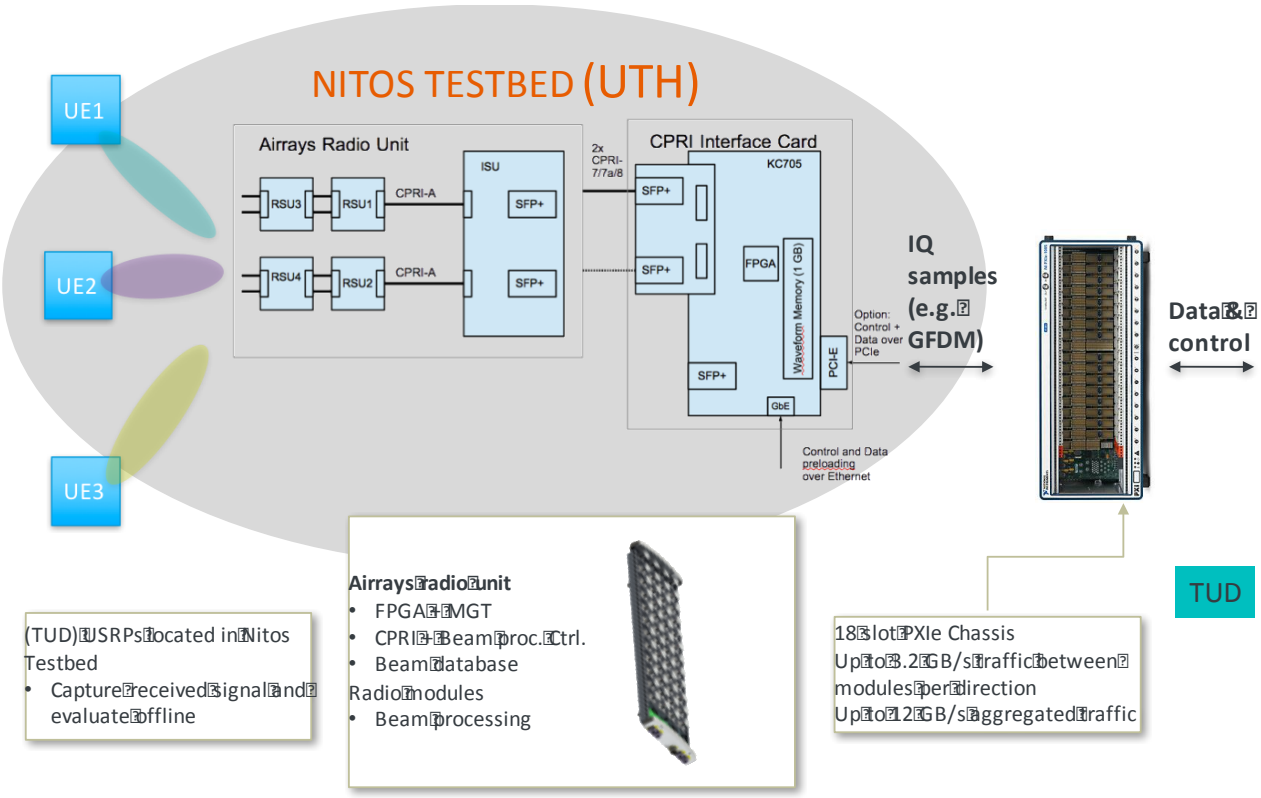

Figure 27: Field trial of GFDM and beamforming using Airrays AAS in the NITOS testbed.

Trial 2: Digital Interconnect for AAS using DWDM

A major challenge for virtual RAN concepts is the large fronthaul capacity required to connect an AAS to a remote (and possibly virtualized) BBU as outlined in Section 2. Depending on the functional split considered, data rate requirements on the transport link can be strongly reduced for the same number of transceivers at the radio unit. Using two optical interconnects, the 5G-XHaul AAS prototype hosts a digital interface with data rates of up to 20 Gbps. Considering the currently implemented Split A architecture, this interface supports up to 16 independent IQ streams, which correspond to 16 virtual antenna ports (compare Figure 2).

One technology to provide very high fronthaul capacity on the same fiber developed in the project is DWDM. The second trial aims at a joint demonstration of the functionality of a DWDM transport system developed by 5G-XHaul partner ADVA and the AAS platform developed by partner Airrays. Up to 16 digital IQ streams are transmitted through a single DWDM fiber and received by the AAS and then internally mapped onto 96 transceivers. The setup that is currently considered is depicted in Figure 28. The concrete integration into the BIO testbed is subject to ongoing activities in 5GX-Haul WP5 and not reported here.

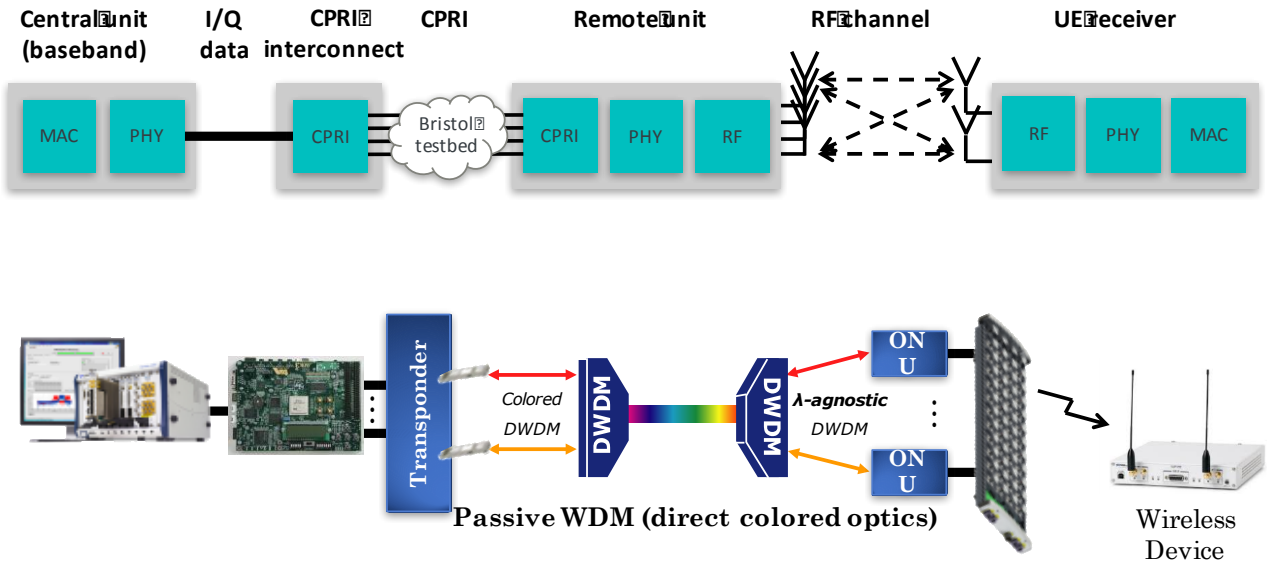

Figure 28: Combined field trial of DWDM and the AAS planned for 2017 in the Bristol testbed.

6 References

[1] E.G. Larsson, O. Edfors, F. Tufvesson and T.L. Marzetta, “Massive MIMO for next generation wireless systems”, *IEEE Communications Magazine*, vol. 52, no. 2, pp. 186-195, 2014.

[2] 5G-XHaul, Deliverable D2.1 – Requirements Specifications and KPIs Document, November 2015, [Online]. Available: http://www.5g-xhaul-project.eu/download/5G-XHaul_D_21.pdf. Accessed Dec. 5, 2016.

[3] 5G-XHaul, Deliverable D2.2 – System Architecture Definition, July 2016, [Online]. Available: http://www.5g-xhaul-project.eu/download/5G-XHaul_D_22.pdf. Accessed Dec. 5, 2016.

[4] P. Harris et al., “LOS Throughput Measurements in Real-Time with a 128-Antenna Massive MIMO Testbed”, IEEE Global Communications 2016, Washington D.C., Dec. 2016.

[5] E. Luther, “5G Massive MIMO Testbed: From Theory to Reality”, white paper, available online: https://studylib.net/doc/18730180/5g-massive-mimo-testbed--from-theory-to-reality

[6] 3GPP, TR 38.913: Study on Scenarios and Requirements for Next generation Access Technologies, 3GPP Technical Report, 2016.

[7] Common Public Radio Interface, http://www.cpri.info/. Accessed Aug. 1, 2016.

[8] U. Dötsch et al., “Quantitative Analysis of Split Base Station Processing and Determination of Advantageous Architectures for LTE”, *Bell Labs Tech. J.*, vol. 18, no 1, pp. 105–128, 2013.

[9] D. Wübben et al., “Benefits and Impact of Cloud Computing on 5G Signal Processing”, *IEEE Signal Process. Mag.*, vol. 31 no. 6, pp. 35-44, 2014.

[10] G. Wunder et al., "5GNOW: non-orthogonal, asynchronous waveforms for future mobile applications," *IEEE Communications Magazine*, vol. 52, no. 2, pp. 97-105, February 2014.

[11] N. Michailow et al., "Generalized Frequency Division Multiplexing for 5th Generation Cellular Networks," *IEEE Transactions on Communications*, vol. 62, no. 9, pp. 3045-3061, Sept. 2014.

[12] NGMN Alliance, "5G White Paper," 2015. [Online]. Available: http://www.networkworld.com/article/3043500/mobile-wireless/will-5g-say-farewell-to-ofdm.html. Accessed Dec. 4, 2016.

[13] M. Peng, C. Wang, V. Lau and H. V. Poor, "Fronthaul-constrained cloud radio access networks: insights and challenges," *IEEE Wireless Communications*, vol. 22, no. 2, pp. 152-160, April 2015.

[14] M. Majidi, A. Mohammadi and A. Abdipour, "Analysis of the Power Amplifier Nonlinearity on the Power Allocation in Cognitive Radio Networks," *IEEE Transactions on Communications*, vol. 62, no. 2, pp. 467-477, February 2014.

[15] A. Fehske et al. “Smart Large Scale Radio Technology for the Tactile Internet”, final report, H2020 SME Instrument Phase 1, Grant 674292

7 Acronyms

Acronym	Description
3GPP	Third Generation Partnership Project
AAS	Advanced antenna system
ACLR	Adjacent channel leakage ratio
BBU	Base band unit
BER	Bit-error-rate
BH	Backhaul
CAPEX	Capital expenditure
CP-OFDM	Cyclic prefix orthogonal frequency division multiplexing
CPRI	Common public radio interface
C-RAN	Cloud radio access network
CU	Central unit
DUT	Device under test
DWDM	Dense wavbelength division multiplexing
EVM	Error vector magnitude
FH	Fronthaul
f-OFDM	Filtered OFDM
GFDM	Generalized frequency division multiple access
ISU	Interface subunit
LTE	Long term evolution
mmWave	Millimeter wave
MIMO	Multiple-input-multiple-output
OOB	Out-of-band
PA	Power amplifier
PN	Phase noise
RRH	Remote radio head
RU	Radio unit
RSU	Radio subunit
SDR	Software defined radio